REPORT DOCUMENTATION PAGE

Form Approved
OMB No. 0704-0188

1. REPORT DATE *(DD-MM-YYYY)*	**2. REPORT TYPE**	**3. DATES COVERED** *(From - To)*
28-08-2009	Technical Paper	

4. TITLE AND SUBTITLE

Experimentally Characterizing the Plume of a Divergent Cusped-Field Thruster

5a. CONTRACT NUMBER

5b. GRANT NUMBER

5c. PROGRAM ELEMENT NUMBER

6. AUTHOR(S)
Stephen R. Gildea & Manuel Martinez-Sanchez (Massachusetts Institute of Technology);
Michael R. Nakles (ERC); & William A. Hargus Jr. (AFRL/RZSS)

5d. PROJECT NUMBER

5e. TASK NUMBER

5f. WORK UNIT NUMBER
33SP0706

7. PERFORMING ORGANIZATION NAME(S) AND ADDRESS(ES)

Air Force Research Laboratory (AFMC)
AFRL/RZST
4 Draco Drive
Edwards AFB CA 93524-7160

8. PERFORMING ORGANIZATION REPORT NUMBER

AFRL-RZ-ED-TP-2009-324

9. SPONSORING / MONITORING AGENCY NAME(S) AND ADDRESS(ES)

Air Force Research Laboratory (AFMC)
AFRL/RZS
5 Pollux Drive
Edwards AFB CA 93524-7048

10. SPONSOR/MONITOR'S ACRONYM(S)

11. SPONSOR/MONITOR'S NUMBER(S)
AFRL-RZ-ED-TP-2009-324

12. DISTRIBUTION / AVAILABILITY STATEMENT

Approved for public release; distribution unlimited (PA #09406).

13. SUPPLEMENTARY NOTES
For 31st International Electric Propulsion Conference (IEPC 09) to be held in Ann Arbor, MI from 20-24 September 2009.

14. ABSTRACT

Divergent cusped-field thrusters are electric propulsion devices characterized by a divergent, dielectric wall channel and a magnetic topology dominated by two magnetic cusps and a magnetic bottle near the anode. Initial testing results suggest that this technology may lend itself to miniaturization while providing improved lifetime performance over miniature Hall thruster designs. This paper presents results of detailed probing of the divergent cusped-field thruster plume using a faraday cup and a retarding potential analyzer to measure the ion current density and energy distributions at varied operating conditions. These results provide a more complete experimental characterization of the plume than was previously available by measuring plume attributes at wider angles with increased spatial resolution. Plume data analyses show regions with the greatest current density contain the most energetically uniform ion populations. However, the retarding potential analyzer results indicate that highly energetic ions are expelled at large angles relative to the thruster axis of symmetry, though the current densities at these angles are much lower. Plume measurements made while varying the cathode operating condition are also presented. The operating conditions of the divergent cusped-field thruster and cathode are found to be strongly coupled, motivating a future study that systematically examines the effect of cathode location and operating condition on the performance of the thruster. The mode transitions that occur while operating the divergent cusped-field thruster are also examined, providing a quantitative comparison between the two.

15. SUBJECT TERMS

16. SECURITY CLASSIFICATION OF:			**17. LIMITATION OF ABSTRACT**	**18. NUMBER OF PAGES**	**19a. NAME OF RESPONSIBLE PERSON**
					Dr. William A. Hargus Jr
a. REPORT	**b. ABSTRACT**	**c. THIS PAGE**	SAR	16	**19b. TELEPHONE NUMBER** *(include area code)*
Unclassified	**Unclassified**	**Unclassified**			N/A

Experimentally Characterizing the Plume of a Divergent Cusped-Field Thruster

Stephen R. Gildea*, Manuel Martínez-Sánchez†
Massachusetts Institute of Technology, Cambridge, Massachusetts, 02139, USA

Michael R. Nakles‡ and William A. Hargus, Jr.§
Air Force Research Laboratory Spacecraft Propulsion Branch, Edwards Air Force Base, California, 93524, USA

Divergent cusped-field thrusters are electric propulsion devices characterized by a divergent, dielectric wall channel and a magnetic topology dominated by two magnetic cusps and a magnetic bottle near the anode. Initial testing results suggest that this technology may lend itself to miniaturization while providing improved lifetime performance over miniature Hall thruster designs. This paper presents results of detailed probing of the divergent cusped-field thruster plume using a faraday cup and a retarding potential analyzer to measure the ion current density and energy distributions at varied operating conditions. These results provide a more complete experimental characterization of the plume than was previously available by measuring plume attributes at wider angles with increased spatial resolution. Plume data analyses show regions with the greatest current density contain the most energetically uniform ion populations. However, the retarding potential analyzer results indicate that highly energetic ions are expelled at large angles relative to the thruster axis of symmetry, though the current densities at these angles are much lower. Plume measurements made while varying the cathode operating condition are also presented. The operating conditions of the divergent cusped-field thruster and cathode are found to be strongly coupled, motivating a future study that systematically examines the effect of cathode location and operating condition on the performance of the thruster. The mode transitions that occur while operating the divergent cusped-field thruster are also examined, providing a quantitative comparison between the two. Additionally, time resolved anode current measurements are presented for several operating conditions. These data reveal a distinct difference between the low and high current modes, demonstrating that the anode current is much less oscillatory in the low current mode than the high current mode.

Nomenclature

V_a = Anode potential with respect to ground
$\dot{m}_a$ = Anode mass flow rate
I_k = Keeper current
$\dot{m}_c$ = Cathode mass flow rate

*Graduate Student, Department of Aeronautics and Astronautics, sgildea@mit.edu
†Professor, Department of Aeronautics and Astronautics, mmart@mit.edu
‡Research Engineer, ERC Inc., michael.nakles.ctr@edwards.af.mil
§Research Engineer, AFRL/RZSS, william.hargus@edwards.af.mil

The 31th International Electric Propulsion Conference, Ann Arbor, Michigan, USA, September 20-24, 2009

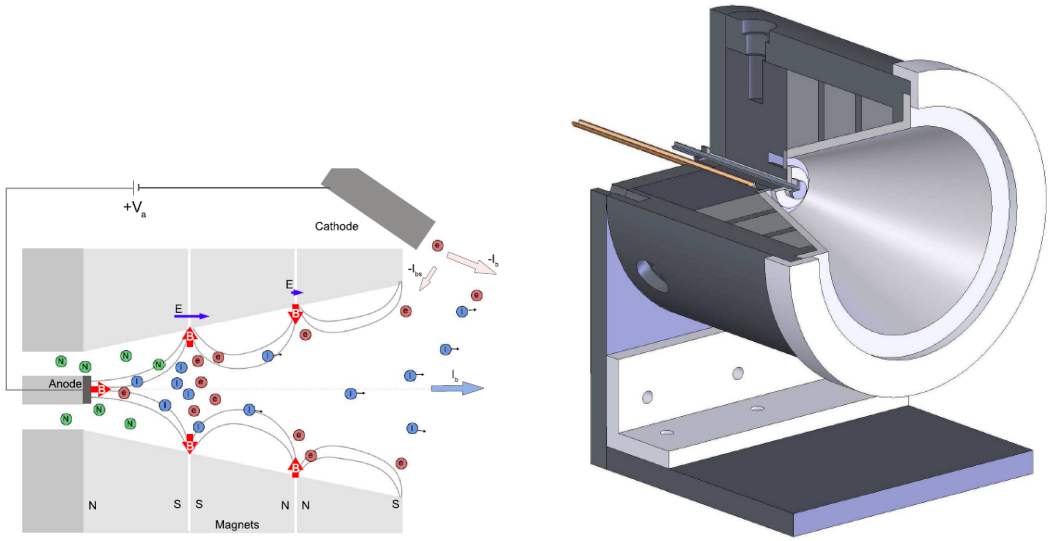

(a) DCFT operating at the MIT SPL.[4]

(b) 3D Engineering Model of DCFT.[5]

Figure 1. DCFT visualizations.

I. Introduction

Stationary plasma type (SPT) Hall thrusters have been operated in earth orbit since 1972[1] with typical efficiencies near 50% and a specific impulse of 1600 s.[2] However, the operational lifetime of SPT Hall thrusters is often limited by erosion of dielectric material used to provide insulation from the plasma.[3] Researchers at the Massachusetts Institute of Technology (MIT) Space Propulsion Laboratory (SPL) began investigating divergent cusped-field (DCF) thrusters[4–6] to determine their promise as a longer lifetime alternative to existing low power Hall thrusters. Other cusped-field thrusters include the High Efficiency Multi-stage Plasma (HEMP) thrusters patented by THALES Electron Devices[7–9] and the Cylindrical Hall Thruster (CHT) developed at the Princeton University Electric Propulsion & Plasma Dynamics Laboratory.[10] A detailed comparison of the DCFT design to the HEMP, CHT, and other cusped-field devices is provided by Courtney *et al.*[6]

A. Divergent Cusped-Field Thruster (DCFT)

DCF thrusters are electric propulsion devices characterized by a divergent, dielectric wall channel and a magnetic topology dominated by two magnetic cusps and a magnetic bottle near the anode. The magnetic circuit consists of three annular samarium cobalt (SmCo) permanent magnets arranged such that like poles face one another, and a core at the base of the thruster composed of 1018 carbon steel (see Figures 1(a) and 1(b)). Xenon gas is injected 5 mm upstream from the downstream face of the anode through a porous, stainless steel disc embedded in the magnetic core. In this way, the neutral injection and anode locations are decoupled from one another in the DCFT design. For complete details of the DCFT and existing data, please consult previous studies.[4–6,11–13]

Existing experimental data[4–6] catalogues DCFT performance (anode specific impulse, thrust, anode thrust efficiency) at operating conditions ranging between 100 W to 500 W, with a nominal operating condition corresponding to a xenon flow rate of 8.5 sccm and an applied anode voltage of 550 V. At this operating point, the DCFT consumes 242 W of power, and produces 13.4 mN of thrust while operating with an anode thrust efficiency of 44.5%. Although basic DCFT operating principles are thought to include azimuthal electron currents within regions characterized by radial magnetic fields, the competing roles that strong magnetic bottles and internal electric fields play in determining the location and efficiency of ionization (whether in the upstream cusp, downstream cusp, or both) have yet to be explicitly measured in experiments or rigourously explained based on theoretical arguments or simulation results. Demonstrating the effectiveness of the magnetic topology and divergent chamber geometry as erosion barriers remains unachieved as well.

The 31th International Electric Propulsion Conference, Ann Arbor, Michigan, USA, September 20-24, 2009

The present investigation provides detailed probing results of the DCFT plume using a Faraday Cup (FC) and a Retarding Potential Analyzer (RPA) to measure the ion current density and energy distributions at different flow rates and applied voltages. FC and RPA results are presented for several operating conditions, including cases where the cathode flow and power were altered to study the affect of these changes on visible and measured plume structure. Anode current oscillation measurements are also given.

II. Plume Measurements

The following experiments were performed in Chamber 1 at the Edwards Air Force Base (AFB) Air Force Research Laboratory (AFRL) Space Propulsion Branch. Chamber 1 is a cylindrical non-magnetic stainless steel vacuum chamber with a 2.4 m diameter and a 4.1 m length. Pumping is provided by two liquid nitrogen baffled, 1.2 m flanged gaseous helium two stage cryogenic (15 K) vacuum pumps with a measured pumping speed on both xenon and krypton of 48,500 L/s. An automated 2D (R-Θ) stage was used to move Faraday and RPA probes within the plume of an operating DCF thruster to measure the characteristics of the plasma being ejected. The arm mounted on the rotary stage is a stepper motor drive linear translational stage capable of traversing up to 80 cm from the center of rotation of the rotary stage. This combination of rotary and linear motion allows for the continuous sweeping of various plasma interrogation probes in the R-Θ plane. Further details of the probes and experimental facilities are provided by Nakles *et al.*[14] Figures 3(a) and 3(b) show the thruster firing at the Edwards AFB AFRL, and Figure 2 illustrates the coordinate system used to present the probe dat. Thermocouples located on the thruster exterior near the anode and outer case enclosing the permanent magnets indicated that the temperature did not exceed 200°C at those locations during all tests performed for this investigation. Measured chamber pressure did not exceed 3.5 μTorr.

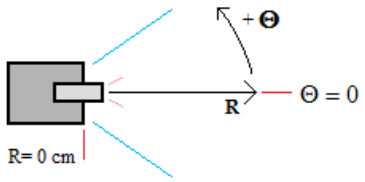

Figure 2. Top view of the 2D (R-Θ) coordinate system. The $\Theta = 0$ line is aligned with the DCFT axis of symmetry. The cathode is above the probing plane, as seen is Figures 3(a) and 3(b).

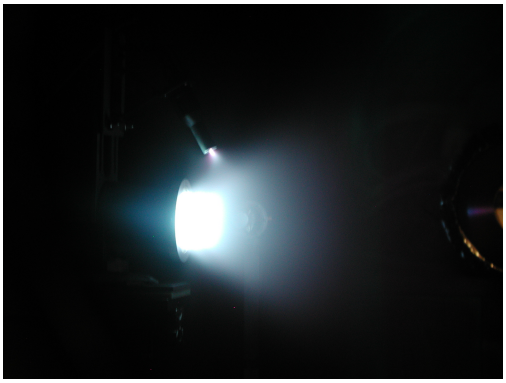

(a) DCFT operating in the high current, or diffuse, mode.

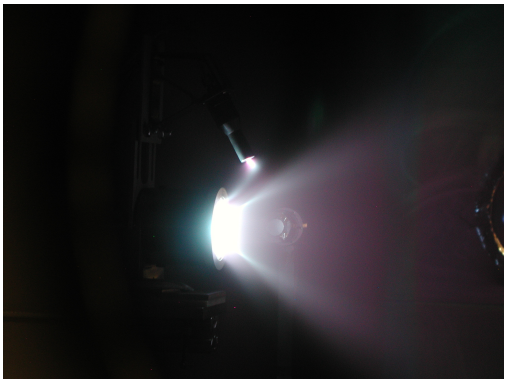

(b) DCFT operating in the low current, or columnated, mode.

Figure 3. A visual comparison of the DCFT plume in two distinct modes, operating at the Edwards AFB AFRL.

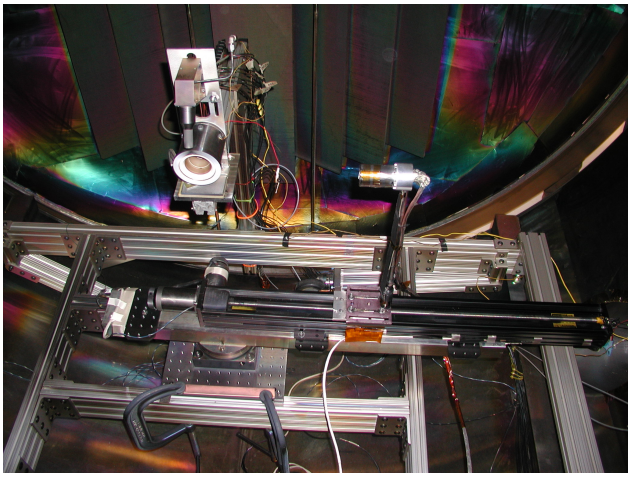

Figure 4. RPA mounted and aligned to measure ion energy distributions within the DCFT plume.

A. RPA Probing

This section presents RPA results for the different operating conditions, presented in Figures 5(a) through 9(f). The RPA data are angularly resolved from $\pm 90^o$ or $\pm 120^o$ off axis in 5^o intervals in both directions, taken at two different radii from the thruster exit plane at each condition.

The 31th International Electric Propulsion Conference, Ann Arbor, Michigan, USA, September 20-24, 2009

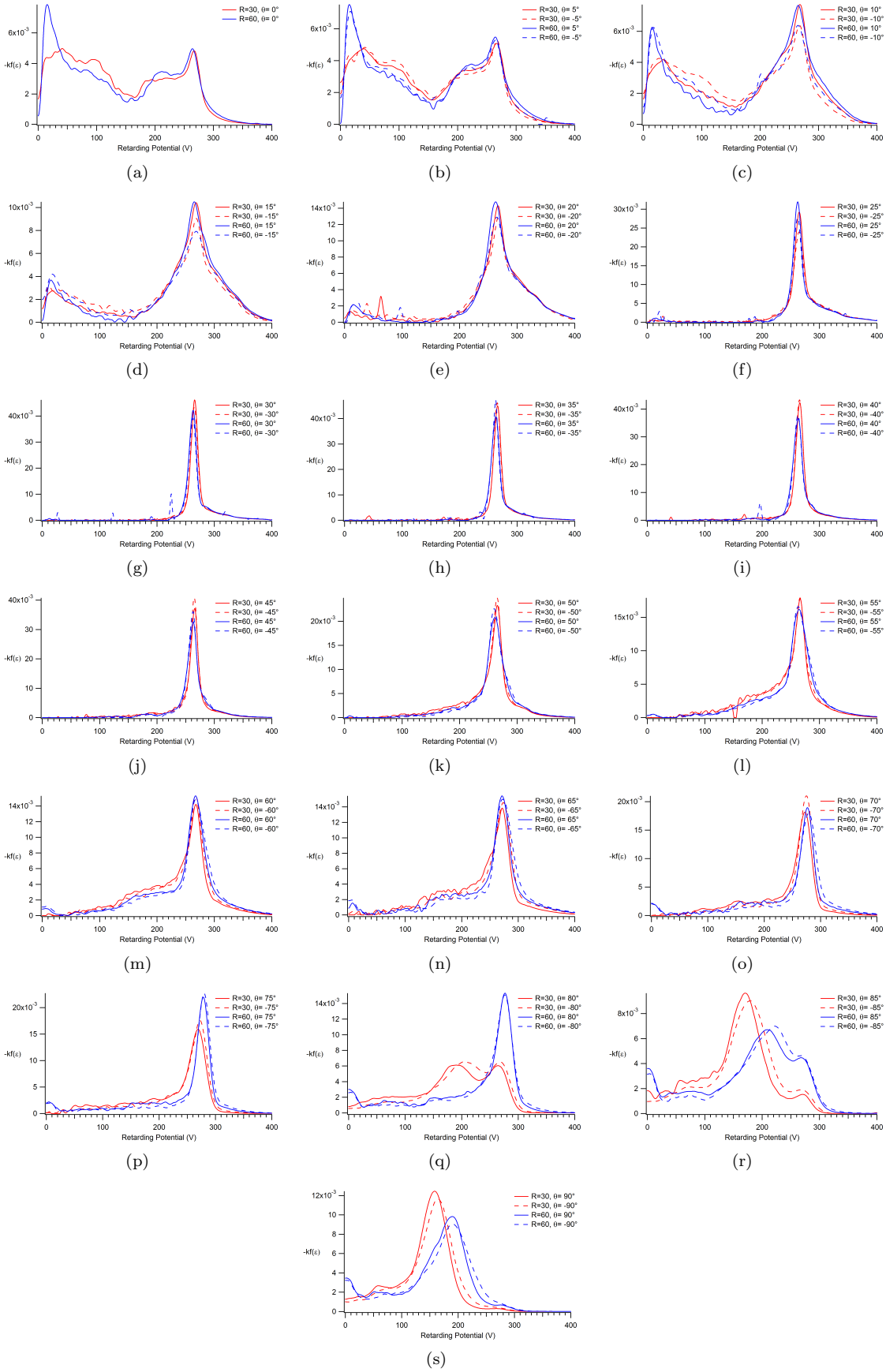

Figure 5. Ion energy distributions plotted at varying positions with respect to the DCFT exit plane. Operating condition: $V_a = 300$ V, $\dot{m}_a = 8.5$ sccm, $I_k = 0.25$ A, $\dot{m}_c = 1.0$ sccm. The units of all radial distances are given in centimeters.

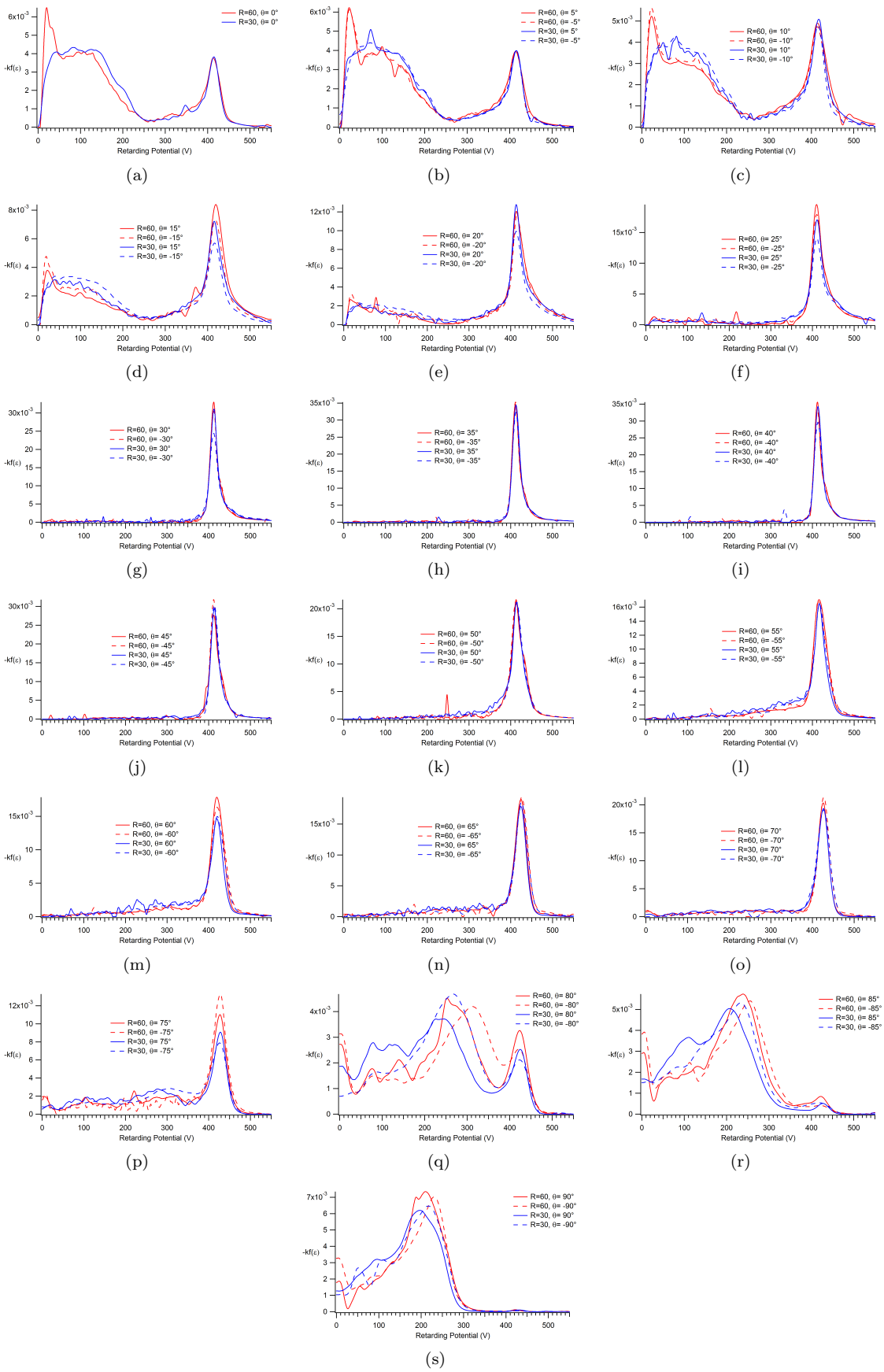

Figure 6. Ion energy distributions plotted at varying positions with respect to the DCFT exit plane. Operating condition: $V_a = 450$ V, $\dot{m}_a = 8.5$ sccm, $I_k = 0.25$ A, $\dot{m}_c = 1.0$ sccm. For angles outside of $\pm 90^\circ$ at this operating condition, see Figures 8(a)-8(f). The units of all radial distances are given in centimeters.

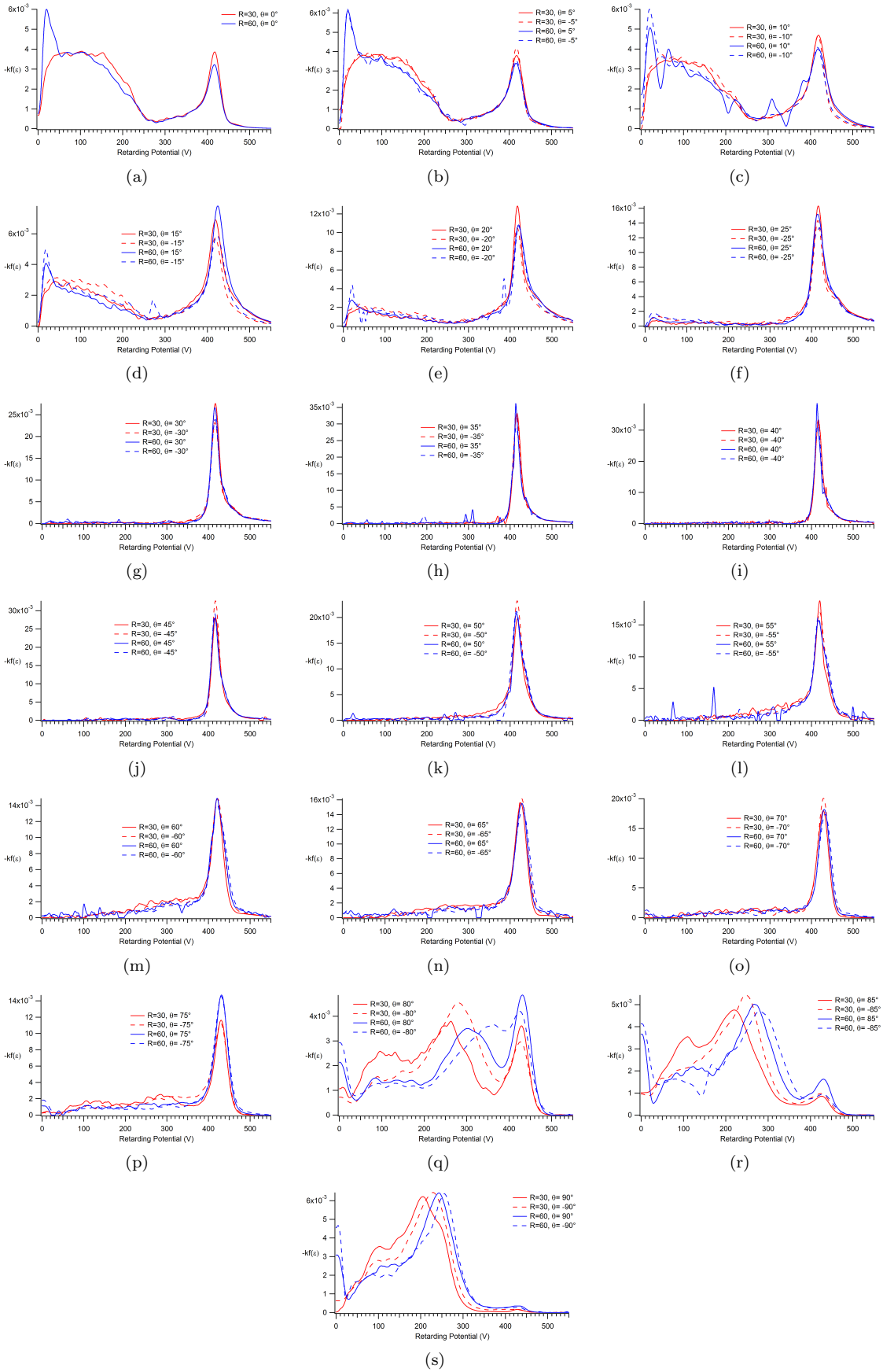

Figure 7. Ion energy distributions plotted at varying positions with respect to the DCFT exit plane. Operating condition: V_a = 450 V, $\dot{m}_a$ = 8.5 sccm, I_k = 0.25 A, $\dot{m}_c$ = 1.0 sccm. For angles of magnitude greater than 90° at this operating condition, see Figures 9(a)-9(f). The units of all radial distances are given in centimeters.

The 31th International Electric Propulsion Conference, Ann Arbor, Michigan, USA, September 20-24, 2009
Distribution A: Approved for public release; distribution unlimited.

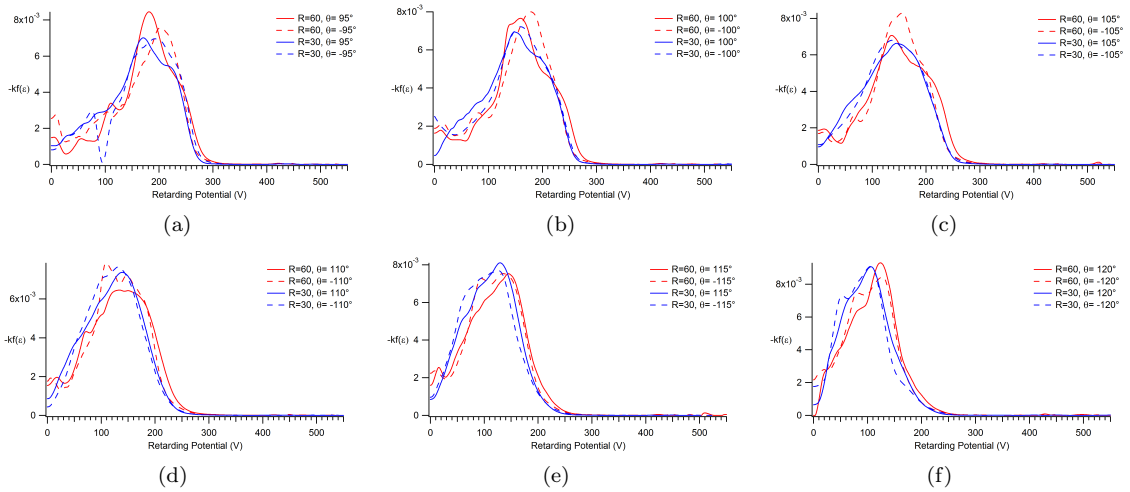

Figure 8. Ion energy distributions plotted at varying positions with respect to the DCFT exit plane. Operating condition: $V_a = 450$ V, $\dot{m}_a = 8.5$ sccm, $I_k = 0.25$ A, $\dot{m}_c = 1.0$ sccm. For angles outside of $\pm$ 90° at this operating condition, see Figures 6(a)-6(s). The units of all radial distances are given in centimeters.

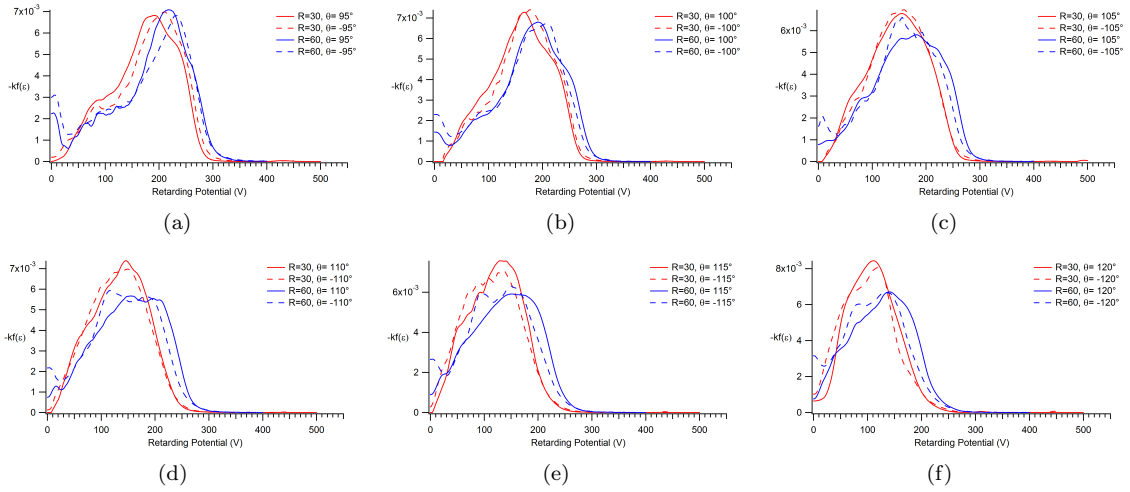

Figure 9. Ion energy distributions plotted at varying positions with respect to the DCFT exit plane. Operating condition: $V_a = 450$ V, $\dot{m}_a = 8.5$ sccm, $I_k = 0.5$ A, $\dot{m}_c = 1.0$ sccm. For angles of magnitude less than 90° at this operating condition, see Figures 7(a)-7(s). The units of all radial distances are given in centimeters.

The 31th International Electric Propulsion Conference, Ann Arbor, Michigan, USA, September 20-24, 2009

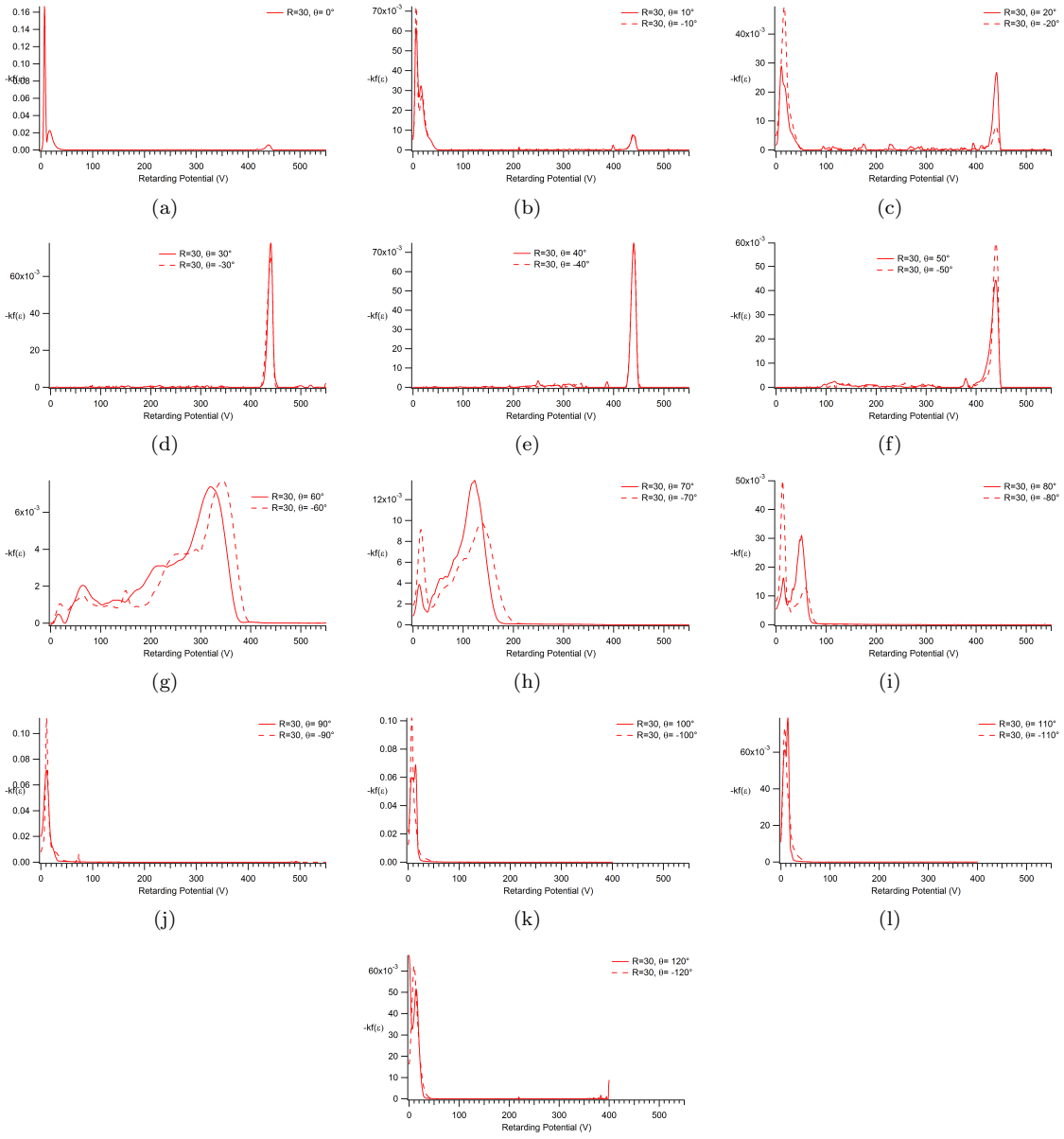

Figure 10. Ion energy distributions plotted at varying positions with respect to the DCFT exit plane. Operating at $V_a = 451$ V, $\dot{m}_a = 4.3$ sccm, $I_k = 0.8$ A, $\dot{m}_c = 2.0$ sccm.

The 31th International Electric Propulsion Conference, Ann Arbor, Michigan, USA, September 20-24, 2009

B. Current Density

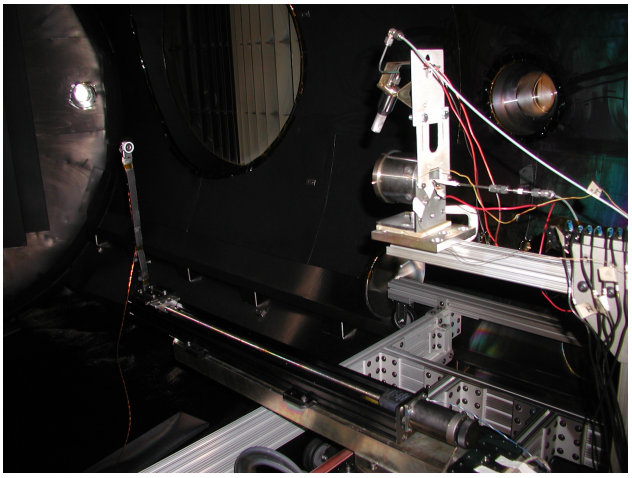

Figure 11. Faraday Cup mounted and aligned to measure current density within the DCFT plume.

This section contains the faraday cup results for the different operating conditions, plotted as the current per steradian. The data are given in Figures 12 through 14. The FC data are angularly resolved from $\pm 120^o$ off axis in 1^o intervals in both directions, taken at two different radii from the thruster exit plane at each condition.

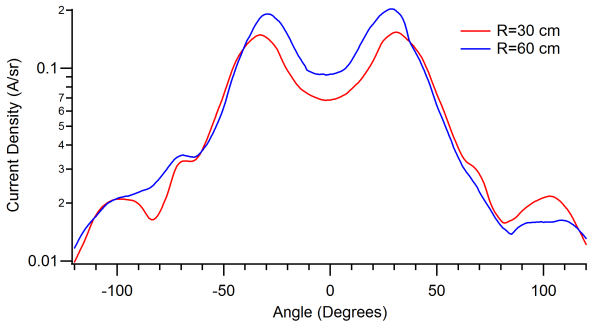

Figure 12. Ion current density distributions plotted at varying positions with respect to the DCFT exit plane. Operating condition: $V_a = 300$ V, $\dot{m}_a = 8.5$ sccm, $I_k = 0.25$ A, $\dot{m}_c = 1.0$ sccm.

The 31th International Electric Propulsion Conference, Ann Arbor, Michigan, USA, September 20-24, 2009

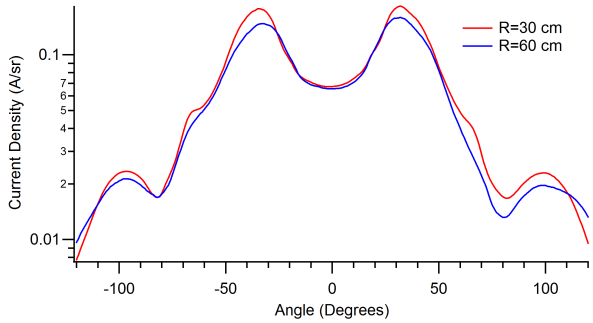

Figure 13. Ion current density distributions plotted at varying positions with respect to the DCFT exit plane. Operating condition: V_a = 450 V, $\dot{m}_a$ = 8.5 sccm, I_k = 0.25 A, $\dot{m}_c$ = 1.0 sccm.

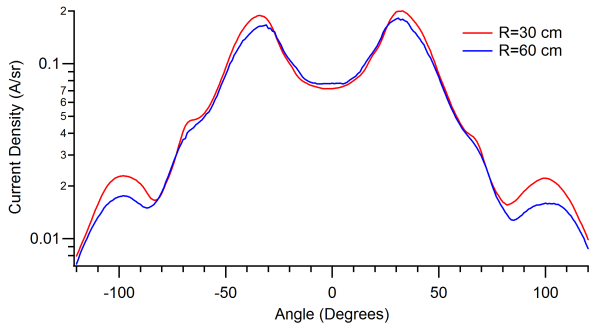

Figure 14. Ion current density distributions plotted at varying positions with respect to the DCFT exit plane. Operating condition: V_a = 450 V, $\dot{m}_a$ = 8.5 sccm, I_k = 0.5 A, $\dot{m}_c$ = 1.0 sccm.

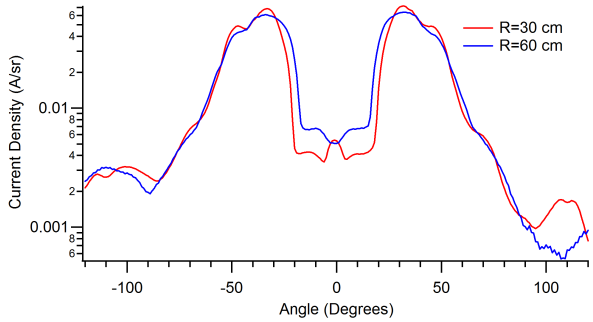

Figure 15. Ion current density distributions plotted at varying positions with respect to the DCFT exit plane. Operating condition: V_a = 475.7 V, $\dot{m}_a$ = 5.8 sccm, I_k = 1.48 A, $\dot{m}_c$ = 1.0 sccm.

III. Current Oscillation Measurements

This section presents the time resolved anode current as recorded with an oscilloscope and processed with a signal analyzer. They demonstrate a conspicuous difference between the anode current behavior in the high and low current modes. The anode currents shown in Figures 16(a) through 16(f), representing the DCFT operating in the high current mode, are characterized by high magnitude, low frequency oscillations. For all high current operating conditions, the lowest harmonic of the frequency spectrum is between 3.5 kHz and 4.0 kHz. The flight time of a neutral Xenon particle with a temperature of 1000 K is approximately 0.2 ms. The frequency corresponding to the inverse of this time is 5 kHz. The anode currents shown in Figures 17(a) through 17(f), representing the DCFT operating in the low current mode, do not exhibit the same oscillatory behavior as seen in the high current mode. The large oscillations present in the high current mode are reduced by several orders of magnitude. Previously,[4,5] the low current mode was found to be the more efficient of the two modes. The lack of strong plasma oscillations in the low current mode further suggest that it is the preferred mode of operation.

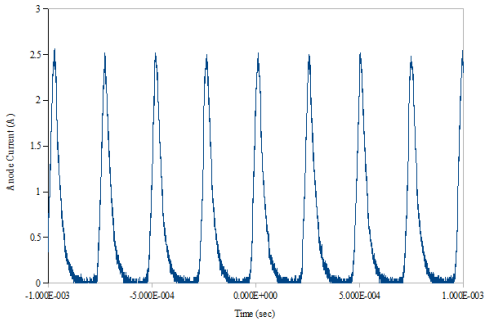

(a) Time resolved anode current. Operating condition: V_a = 300 V, $\dot{m}_a$ = 8.5 sccm, I_k = 0.25 A, $\dot{m}_c$ = 1.0 sccm.

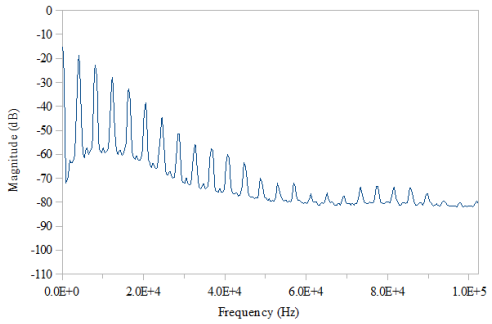

(b) Anode current spectrum. Operating condition: V_a = 300 V, $\dot{m}_a$ = 8.5 sccm, I_k = 0.25 A, $\dot{m}_c$ = 1.0 sccm.

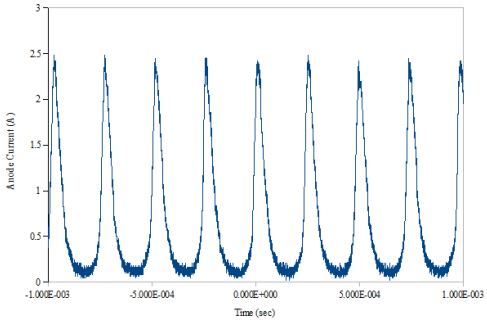

(c) Time resolved anode current. Operating condition: V_a = 450 V, $\dot{m}_a$ = 8.5 sccm, I_k = 0.25 A, $\dot{m}_c$ = 1.0 sccm.

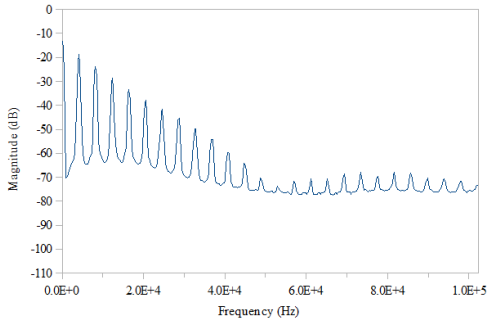

(d) Anode current spectrum. Operating condition: V_a = 450 V, $\dot{m}_a$ = 8.5 sccm, I_k = 0.25 A, $\dot{m}_c$ = 1.0 sccm.

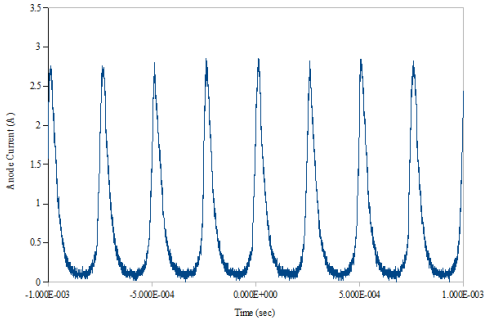

(e) Time resolved anode current. Operating condition: V_a = 450 V, $\dot{m}_a$ = 8.5 sccm, I_k = 0.5 A, $\dot{m}_c$ = 1.0 sccm.

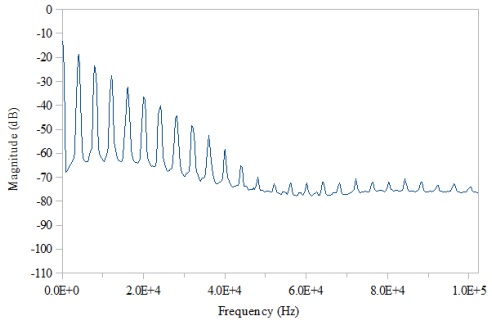

(f) Anode current spectrum. Operating condition: V_a = 450 V, $\dot{m}_a$ = 8.5 sccm, I_k = 0.5 A, $\dot{m}_c$ = 1.0 sccm.

Figure 16. Time resolved anode current and spectrum for the high current mode.

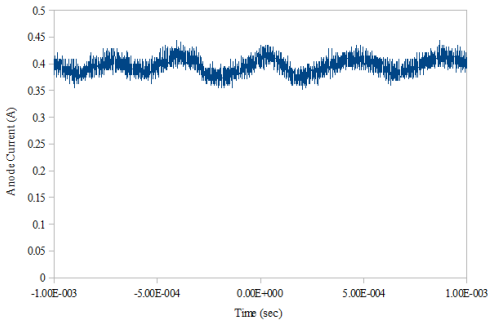

(a) Time resolved anode current. Operating condition: V_a = 450 V, $\dot{m}_a$ = 8.5 sccm, I_k = 0.5 A, $\dot{m}_c$ = 1.0 sccm. This occured while the thruster was warming up, and then transitioned to the high current mode, as in Figure 16(e)

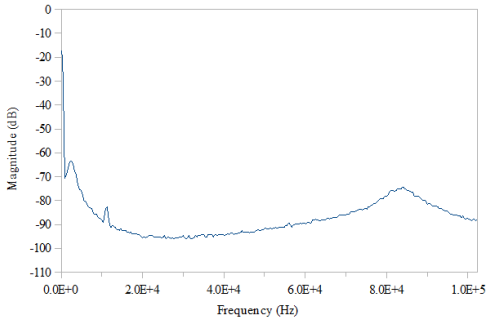

(b) Time resolved anode current. Operating condition: V_a = 450 V, $\dot{m}_a$ = 8.5 sccm, I_k = 0.5 A, $\dot{m}_c$ = 1.0 sccm.

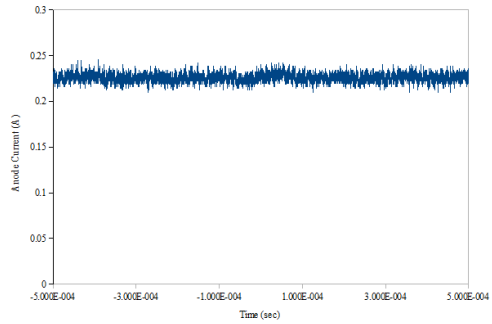

(c) Time resolved anode current. Operating condition: V_a = 450 V, $\dot{m}_a$ = 6.5 sccm, I_k = 1.5 A, $\dot{m}_c$ = 1.0 sccm.

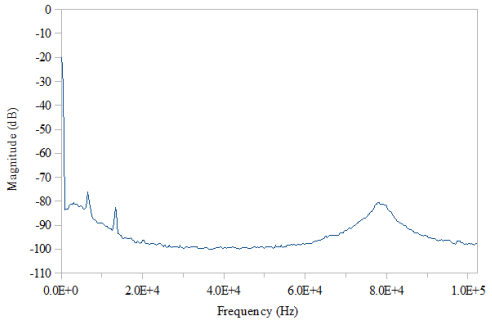

(d) Time resolved anode current. Operating condition: V_a = 450 V, $\dot{m}_a$ = 6.5 sccm, I_k = 1.5 A, $\dot{m}_c$ = 1.0 sccm.

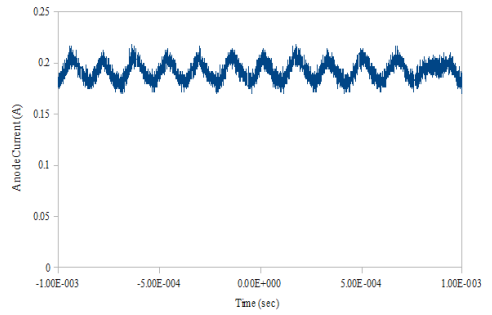

(e) Time resolved anode current. Operating condition: V_a = 475.7 V, $\dot{m}_a$ = 5.8 sccm, I_k = 1.48 A, $\dot{m}_c$ = 1.0 sccm.

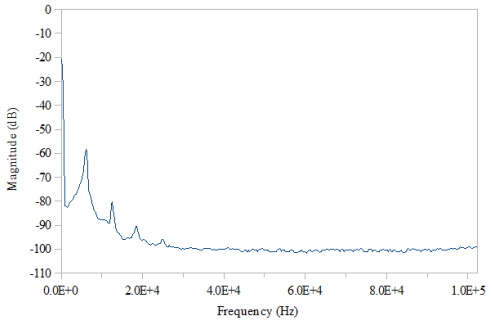

(f) Time resolved anode current. Operating condition: V_a = 475.7 V, $\dot{m}_a$ = 5.8 sccm, I_k = 1.48 A, $\dot{m}_c$ = 1.0 sccm.

Figure 17. Time resolved anode current for the low current mode.

IV. Conclusions & Future Work

The plume measurements expand upon and confirm previous RPA and faraday cup data.[6] A comparison of RPA and Faraday data for identical operating conditions shows that the region of the plume with the greatest current density contains the most energetically uniform ion populations. However, the RPA results indicate that highly energetic ions are expelled at large angles relative to the DCFT axis of symmetry, though the current densities at these angles are much lower. Time resolved anode current data reveal a distinct difference between the low and high current modes. The data demonstrate that the anode current in the low current mode is much less oscillatory than in the high current mode. Identifying the cause of this difference in dynamic behavior will likely contribute toward the determination of basic DCFT operating principles in each mode.

While running the thruster for the purpose of this investigation, the operating conditions of the DCFT and cathode were found to be strongly coupled, motivating a future study that systematically examines the effect of cathode location and operating condition on the performance of the DCFT. A detailed look at the ion energy distributions at high angles in the low current mode would also be beneficial, to determine if high energy ions are as prevalent at high angles in the low current as in the high current mode. Additionally, repeating some of the measurements made hear at different chamber pressures would address the role that charge exchange collisions with background neutrals play in deflecting ions to high angles. However, it is likely that the strong magnetic field outside the thruster is a strong contributor to the high ion energies observed at large plume angles.

Acknowledgements

Paul Adkinson, of the Edwards AFB AFRL, was immensely helpful in the construction, assembly and repair of the anodes used in these experiments. The authors would also like to acknowledge Ryne Barry, an undergraduate student in the Department of Aeronautics & Astronautics at the Massachusetts Institute of Technology, for his assistance in experimental setup and execution. The authors would also like to acknowledge the Science Mathematics And Research for Transformation (SMART) scholarship program for the funding and opportunities that made this project possible. Continuing studies of the divergent cusped-field thruster concept are funded by a grant from the Air Force Office of Scientific Research.

References

[1]Bober, A. S., Kim, V., et al., "State of Works on Electrical Thrusters in the USSR," 22^{nd} *International Electric Propulsion Conference*, Viareggio, Italy, October 1991, also IEPC-91-003.

[2]Martínez-Sánchez, M. and Pollard, J. E., "Spacecraft Electric Propulsion - An Overview," *Journal of Propulsion and Power*, Vol. 14, No. 5, 1998, pp. 688–699.

[3]Kim, V., "Main Physical Features and Processes Determining the Performance of Stationary Plasma Thrusters," *Journal of Propulsion and Power*, Vol. 14, No. 5, 1998, pp. 736–743.

[4]Courtney, D. G. and Martínez-Sánchez, M., "Diverging Cusped-Field Hall Thruster (DCHT)," 30^{th} *International Electric Propulsion Conference*, FLorence, Italy, September 2007, also IEPC-2007-39.

[5]Courtney, D. G., "Development and Characterization of a Diverging Cusped Field Thruster and a Lanthanum Hexaboride Hollow Cathode," S.M. Thesis, Massachusetts Institute of Technology, Cambridge, MA, June 2008.

[6]Courtney, D., Lozano, P., and Martínez-Sánchez, M., "Continued Investigation of Diverging Cusped Field Thruster," 44^{th} *Joint Propulsion Conference & Exhibit*, Hartford, CT, July 2008, also AIAA-2008-4631.

[7]Kornfeld, G., Koch, N., and Coustou, G., "First Test Results of the HEMP Thruster Concept," 28^{th} *International Electric Propulsion Conference*, Toulouse, France, March 2003, also IEPC–03–134.

[8]Kornfeld, G., "Plasma Accelerator Arrangement," United States Patent 6,523,338 B1, 2003.

[9]Kornfeld, G., Coustou, G., and Emsellem, G., "Plasma Accelerator System," United States Patent 7,075,095 B2, 2006.

[10]Raitses, Y. and Fisch, N. J., "Parametric Investigations of a Nonconventional Hall Thruster," *Physics of Plasmas*, Vol. 8, No. 5, 2001.

[11]Matlock, T. et al., "Spectroscopic and Electrostatic Investigation of the Diverging Cusped-Field Thruster," 45^{th} *Joint Propulsion Conference & Exhibit*, Denver, Co, August 2009, also AIAA-2009-4813.

[12]Gildea, S., Batishchev, O., and Martínez-Sánchez, M., "Fully Kinetic Modeling of Divergent Cusped-Field Thrusters," 45^{th} *Joint Propulsion Conference & Exhibit*, Denver, Co, August 2009, also AIAA-2009-4814.

[13]Gildea, S., "Fully Kinetic Modeling of a Divergent Cusped Field Thruster," M. Sc. Thesis Project, Massachusetts Institute of Technology, Cambridge MA, May 2009.

[14]Nakles, M., Barry, R., Larson, C. W., and Hargus, W. A., "A Plume Comparison of Xenon and Krypton Propellant on a 600 W Hall Thruster," 31^{st} *International Electric Propulsion Conference*, Ann Arbor, MI, September 2009.